

District-scale surface temperatures generated from high-resolution longitudinal thermal infrared images

Subin Lin¹, Vasantha Ramani¹, Miguel Martin¹, Pandarasamy Arjunan¹, Adrian Chong², Filip Biljecki^{4,5}, Marcel Ignatius⁴, Kameshwar Poolla³, Clayton Miller^{2*}

¹*Berkeley Education Alliance for Research in Singapore, CREATE Tower 1 Create 6 Way, 138602, Singapore*

²*Department of the Built Environment, College of Design and Engineering, National University of Singapore, 4 Architecture Drive, 117566, Singapore*

³*Department of Electrical Engineering and Computer Sciences, University of California, Berkeley, CA, USA*

⁴*Department of Architecture, College of Design and Engineering, National University of Singapore, 4 Architecture Drive, 117566, Singapore*

⁵*Department of Real Estate, Business School, National University of Singapore, 15 Kent Ridge Drive, 119245, Singapore*

*Corresponding Author: clayton@nus.edu.sg, +65 81602452

Abstract

The paper describes a dataset that was collected by infrared thermography, which is a non-contact, non-intrusive technique to collect data and analyze the built environment in various aspects. While most studies focus on the city and building scales, the rooftop observatory provides high temporal and spatial resolution observations with dynamic interactions on the district scale. The rooftop infrared thermography observatory with a multi-modal platform that is capable of assessing a wide range of dynamic processes in urban systems was deployed in Singapore. It was placed on the top of two buildings that overlook the outdoor context of the campus of the National University of Singapore. The platform collects remote sensing data from tropical areas on a temporal scale, allowing users to determine the temperature trend of individual features such as buildings, roads, and vegetation. The dataset includes 1,365,921 thermal images collected on average at approximately 10 seconds intervals from two locations during ten months.

Keywords:

Infrared thermography observatory, Built environment, IR dataset

1. Background & Summary

Urban ecosystems are the biggest, most dynamic, and most complicated man-made systems, with millions of people interacting and hundreds of governing bodies [1, 2]. Urban modernization has encouraged a significant portion of the global population to move to urban regions. Consequently, the built environment has grown rapidly, and building energy consumption has increased, which augments the release of CO₂ [3, 4]. Improving energy efficiency has been urged by various sectors [5]. The scientific community has made great efforts to better understand the built environment through various sensing technologies [4], based on the development of computational techniques which enable data collection and analysis in vast quantities [1].

Infrared thermography has been widely used in the built environment for many research purposes [6], such as urban heat island [7, 8], building diagnostics [9, 5, 10], and urban heat fluxes [11]. Infrared thermography can provide images showing the surface temperature of different elements in the built environment with a lower cost and effort compared to other similar kinds of sensor networks [6]. It involves the detection of infrared electromagnetic radiation emitted by the inspected

objects and is commonly used for non-destructive testing, and non-contact diagnostic technology [9, 5]. It is based on an infrared imaging system that has been calibrated to measure the emissive power distribution of surfaces at various temperature ranges. The infrared camera generates a series of two-dimensional, readable thermal images, with different colors and tones representing different temperatures [9, 5]. Different infrared systems were reported to be applied to analyze the built environment at different scales: A satellite is able to collect data at the city scale, an aerial vehicle is mainly used at the city and district scales, a rooftop observatory could be used at the district scale, a drone and other handheld devices are used at the building, and human scales [4]. Many previous and current studies focus on the city scale and building scale and could not show the dynamic interactions on the district scale with high-resolution [4, 1]. Furthermore, urban climate studies have been focusing on the temperate climate zones, especially in North America and Europe, and there is a lack of such studies focusing on the tropical climate zones [12, 13, 14].

This work introduces the first thermal observatory deployed in Singapore, a tropical city, with a multi-modal platform that has the flexibility and high resolution to assess a wide range of dynamic processes in urban systems. The thermal observatory

was set up on the roof of buildings that overlooked several educational buildings on the National University of Singapore campus. The platform gathers remote sensing data from a tropical area at a high temporal resolution at approximately 10 seconds intervals, providing the temperature trends of specific urban elements such as buildings, roads, and vegetation. Demonstration codes were given with data preprocessing, such as segmentation, in order to handle and analyze the generated raw data and allow users to use the data with high flexibility, catering to their research needs.

2. Methods

2.1. Thermal images data collection

Thermal images are taken from a FLIR A300 (9 Hz) thermal camera on top of an urban-scale IR observatory, as shown in Figure 1. The detailed specifications of the thermal camera are listed in Table 1. The thermal camera is protected by a housing against rains with IP67 protection. It was attached to a pan/tilt device that can spin 360° along its horizontal axis to record thermal images in multiple locations. These structures (thermal camera, housing, pan/tilt) were placed on a 2-m-high truss tower to avoid any impediments while taking thermal images. Concrete blocks serve as stabilizing support, and an air terminal serves as lightning protection for the truss tower. Two plugs were added to the truss tower to allow a backup battery in the water tank room to power both the thermal camera and the motor of the pan/tilt device. The backup battery is continually charged from the building's electrical supply to enable the pan/tilt unit and thermal camera to be operational for up to two hours in the event of a power outage. A laptop with a weatherproof casing in the water tank room was also linked to the pan/tilt device and thermal camera for customizing and reviewing the collection of thermal images.

The thermal images are collected from two separate locations, namely Kent Vale and S16. The Kent Vale observatory is located on the rooftop of a 42-m-tall building in a residential area, which is located in front of a university campus consisting of office and educational buildings, in order to access the district-scale analysis. The pan/tilt unit was configured from two separate software to allow the thermal camera to take images from four positions (I, II, III, and IV), as shown in Figure 2. The first software was installed in a video encoder to control the positions of the pan/tilt unit to take a thermal image. The second software developed by NAX Instruments Pte Ltd was installed in the laptop to control the moment to take a thermal image, which could then be saved either in JPEG or FFF file format. Information of four different buildings (Figure 1) can be captured by the observatory with thermal images: A (CREATE), centered by position I, is 68-m-tall with an important portion of its facade covered by curtain walls; B (E1A) and C (EA), centered by position II and III separately, are about 27-m-tall, consists of concrete walls and single-pane windows; D (SDE4), observed in position IV, consists of metal grids installed on a concrete frame, designed to be net-zero building, and its height is around 24 meters. Surface temperatures of

trees are also observed from the above positions. There exists a road with traffic in front of buildings B, C, and D, and the road can be observed in thermal images taken from position IV. The observatory moved from position I to IV sequentially and recorded thermal images at various time intervals. The detailed time for the image taken is shown in its file name. Then, using a 4G Internet connection fitted on the laptop, the captured thermal images are stored on the Google Drive repository.

Image resolution	16 bit, 320 × 240 pixels
Sensor	Uncooled Microbolometer FPA
Thermal sensitivity	50 mK @ 30 °C
Spectral range	7.5 - 13 μm
Field of view (FOV)	25°(H) and 18.8°(V)
Accuracy	±2° or 2% of reading
Camera Weight	0.7 kg
Power supply	110/220 V AC
Size	170mm × 70mm × 70mm

Table 1: Information about the FLIR A300 thermal camera

The S16 observatory is located on the rooftop of a nine-story building in an educational area on a university campus. The pan/tilt unit was first set to take images from three positions (1, 2, and 3), as shown in Figure 4. Information from three different buildings can be captured by the observatory with thermal images (Figure 3). The observatory moved from position 1 to 3 sequentially and record thermal images at various time intervals per view. Various elements could be observed from the captured thermal images, such as air condition units, glass materials, vegetation, and solar panels. These different elements could be further analyzed for various research purposes.

Due to the unstable system adjustment of the second observatory, thermal images taken in the S16 site are not captured in the exact same locations (i.e., they are tilted to the left or right), thus, automated segmentation tools are highly encouraged to address this issue. Furthermore, as there were network issues in the second observatory system on S16, images captured positions were changed to keep the locations as close as possible, as shown in Figure 5.

The thermal camera is made up of an optical system that directs radiation from the scene onto a microbolometer [16]. Long-wave infrared radiation changes the resistance of the detector, which is translated to apparent temperature (T_{obj}) readings as follows [16]:

$$T_{obj} = \frac{B}{\ln\left(\frac{R_1}{R_2(U_{tot}+O)} + f\right)} \quad (1)$$

where U_{tot} is the signal response to the incident long-wave infrared radiation on the detector, B , R_1 , R_2 , O , and f denote the camera calibration constants, which are calibrated by the camera manufacturer and are stored in the thermal image metadata.

2.2. Data preprocessing

Data preprocessing was done prior to the analysis of the images for Kent Vale dataset. First, data filtering was conducted



Figure 1: Observatory installed on the rooftop of the residential area in Singapore and its captured information. Source of the imagery: Google Earth. [15]

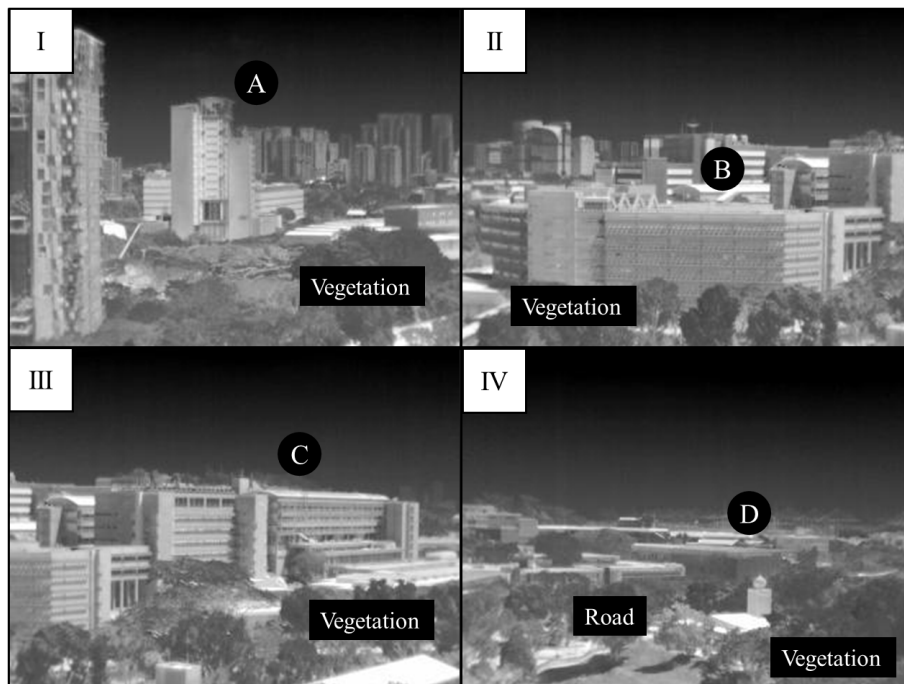


Figure 2: Positions where the observatory capture thermal images on Kent Vale [15]

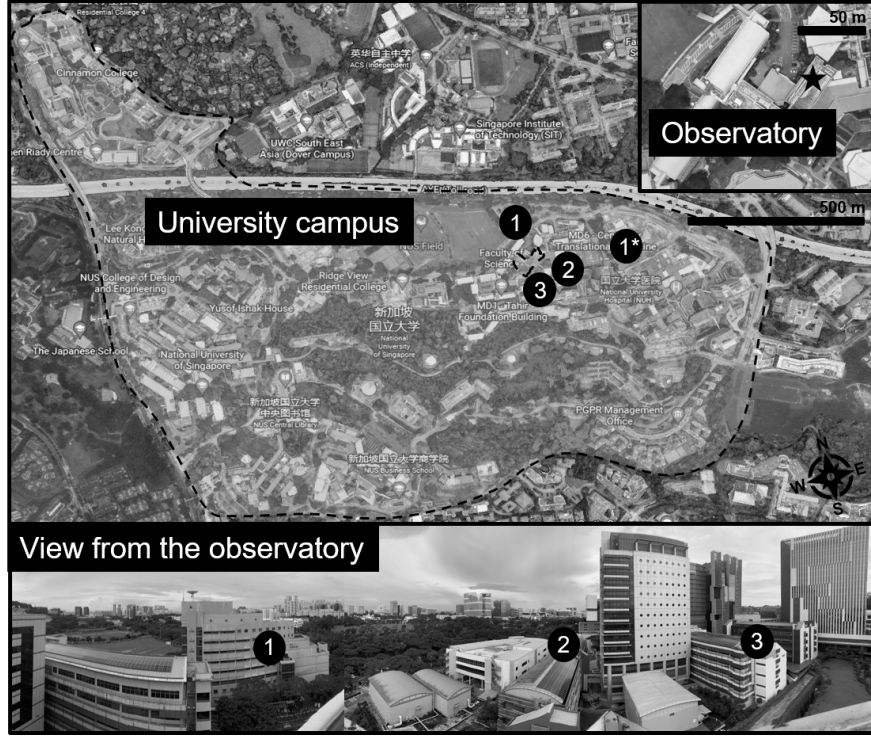


Figure 3: Observatory installed on the rooftop of the university campus in Singapore and its captured information. Source of the imagery: Google Earth.

to remove images that were not suitable for analysis manually. Thermal images captured during the rainy period were disturbed by rain droplets and hence need to be removed. Then, a convolution neural network (CNN) classification model was applied to exclude blurred images that were taken while the pan/tilt unit was moving. The CNN model is also used for the classification of the building type for the first location. The model was trained on 4316 pre-classified images and then be used to classify thermal image datasets of Kent Vale.

2.3. Weather station data collection

The locations of the weather stations are shown in Figure 6. The weather stations measured meteorological data in multiple locations on the university campus at around 2 m above the ground, except for locations 1 and 7, which are on rooftops. The six recorded parameters are air temperature ($^{\circ}\text{C}$), relative humidity (RH, %), dew point ($^{\circ}\text{C}$), wind speed (m/s) and direction (degree), gust speed (m/s), and solar radiation (W/m^2) at a 1-minute interval. For location 9, only the first three parameters were recorded. The weather stations were calibrated before installation. The specification of the weather stations is listed in Table 2. Details of the weather station installment are available in Chen et al.[17], and Yu et al.[18].

3. Data Records

The thermal image data and the weather station data for the same periods are published in Zenodo with open access [20]. The thermal images dataset contains two locations: Kent Vale and S16. 483915 thermal images were taken from

Kent Vale between November 8, 2021, and March 8, 2022. 882006 thermal images were taken from S16 between August 3, 2022, and December 14, 2022. The images taken time are indicated in their file names. The data were converted and stored in JPEG format. The thermal images were stored in folders according to locations and views and listed in sequential order. The detailed hierarchy of the data folders is listed in the data/README file on GitHub (<https://github.com/buds-lab/project-iris-dataset>). An example of the data folder hierarchy: 2022-08-03/view_1/smap-2022-08-03T13-48-18.19.jpeg. Missing values are intended, as the preprocessing process filters unsuitable images for analysis. The images taken at Kent Vale were classified by the CNN model into five different groups: CREATE (I), E1A (II), EA (III), SDE4 (IV), and Corrupted. The Corrupted group collected images that were not classified into any of the above four views, which means that these collected images were of low quality and unable to be distinguished; hence needed to be excluded. The summary of the provided dataset is shown in Table 3. The code structure demonstration is also available in Readme in the GitHub link: <https://github.com/buds-lab/project-iris-dataset>. The code demonstration contains three subcategories: data, notebook, and src. The data directory shows all the original data and converted/processed data; The notebook directory includes three notebooks contain three preprocess steps; and the src directory runnable preprocessing scripts. The weather station data is provided in excel format. It contains some missing values, therefore prior data preprocessing is needed.

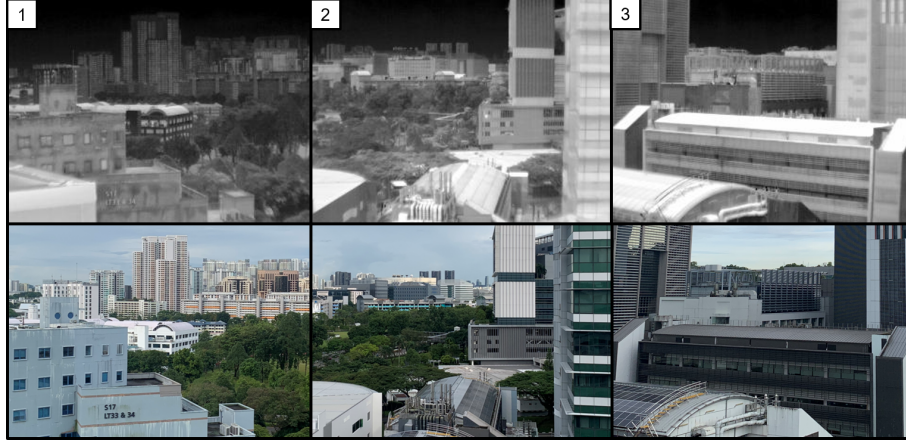


Figure 4: Positions where the observatory capture thermal images on S16

Duration	Parameter	Temperature	Solar Radiation	Wind Speed
01/11/2021 - 08/03/2022 01/08/2022 - 14/12/2022	Range	-40°C-75°C	0-1280 W/m ²	0-50 m/s
	Accuracy	± 0.21 °C	±10 W/m ²	0.2 m/s
	Resolution	0.01 °C	1.25 W/m ²	0.2 m/s

Table 2: Specifications of weather station sensors [18]

4. Technical Validation

4.1. Sensitivity analysis

Prior to evaluating the infrared receptor (T_{ij}) from the observatory, a sensitivity analysis on factors that might have a significant impact on its variance was carried out. First-order Sobol index [21] was used to estimate the contribution of a variable to the variance of T_{ij} . The total Sobol index was also computed in order to consider the interactions between variables.

During the sensitivity analysis, the variables and their corresponding constraints are measured and shown in Table 2 4 [15]. The Satteli sampler [22] on thermal images taken at the four positions during a sunny day in Singapore was used to calculate the first order and total Sobol indices. T_{ij} was determined for each sample at various times of the day and thermal camera placements. The sensitivity of each variable at different periods was given using the mean indices across the four positions.

4.2. Parameters calibration

The thermal images' surface temperature estimates were calibrated in accordance with the information gathered by contact surface sensors, as shown in Figure 7 at three different positions. Between December 2021 and March 2022, a heat flux (HF) sensor and a temperature probe were installed at Position a on the surface of a window in Building B. Both the HF sensor and the temperature probe were connected to a Hioki data logger and measured the surface temperature every 3 seconds. Another type of data logger, UbiBot WS1 pro indoor monitoring sensor, was used to connect temperature probes at position b and c , respectively.

The output voltage recorded by the infrared receptor at position ij in the thermal image is represented by an array U_{ij}^r and

a header in these files. Equation 2 can be used to transform U_{ij}^r into longwave radiations (L_{ij}^r) between 7.5 and 13 micrometers:

$$U_{ij}^r = cL_{ij}^r \quad (2)$$

where c is a constant.

The FLIR A300 (9 Hz) thermal camera that was installed in the observatory was calibrated such that the following Equation 3 holds true for the surface temperature of a target element detected by the infrared receptor (T_{ij}^r):

$$T_{ij}^r = g(U_{ij}^r) = b \ln \left[\frac{r_1}{r_2(U_{ij}^r + O)} + f \right]^{-1} \quad (3)$$

where b , r_1 , r_2 , O , and f are calibrated parameters.

However, the parameters in Equation 3 need to be calibrated in order to minimize the discrepancy between T_{ij}^r and T_{ij} in an outdoor environment. In this case, these values are acquired in a controlled setting where the target element's actual surface temperature T_{ij} at location ij in the thermal picture is almost identical to T_{ij}^r .

The FLIR A300 camera was calibrated by manually tuning the parameters in Equation 3 until there was a satisfactory level of agreement between surface temperature estimations and observations. The agreement was assessed in terms of the Mean Bias Error (MBE) and Root Mean Square Error (RMSE) as shown in Equation 4 and 5:

$$MBE = \frac{1}{n} \sum_{i=1}^n (T_S^n - T_{S,m}^n) \quad (4)$$

$$RMSE = \sqrt{\frac{1}{n} \sum_{i=1}^n (T_S^n - T_{S,m}^n)^2} \quad (5)$$

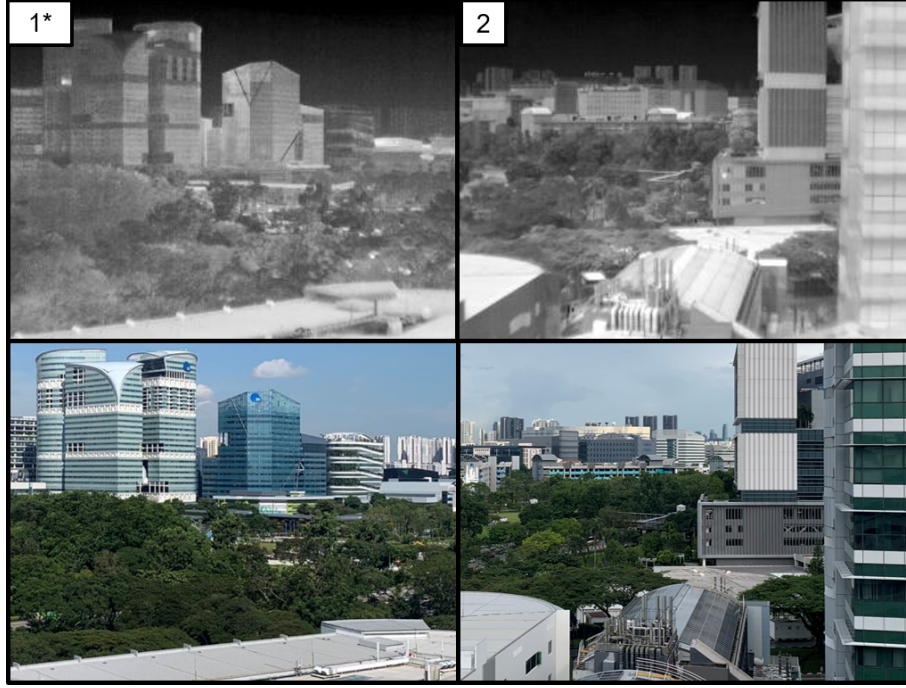


Figure 5: Positions where the observatory capture thermal images on S16 after adjustment

Duration	Resolution (sec)	Locations	Views	Examples	Corrupted size	Dataset size
08/11/2021-08/03/2022	vary	Kent Vale	I	72036	100758	483915
			II	96289		
			III	127506		
			IV	87326		
03/08/2022-14/12/2022	vary	S16	no classify	/	/	882006

Table 3: Summary of the provided datasets at each location: duration of each location, number of views per group, the number of examples per view, corrupted size per view and dataset size

where $T_{S,m}^n$ is the surface temperature obtained by contact surface sensors, and T_S^n is the surface temperature calculated from thermal pictures captured by the FLIR A300 camera at time $t = t_0 + n \cdot \Delta t$. The calibration aims to achieve an MBE as close to 0 with the lowest RMSE. The RMSE and MBE were calculated with different Δt at different positions (30 minutes at Position A and 5 minutes for Positions B and C).

5. Usage Notes

5.1. Factors consideration

When evaluating T_{ij} from the rooftop observatory, several factors have to be taken into account. First, the buildings, streets, and trees which could be seen from the observatory are exposed to longwave radiations mainly coming from the sky-dome. Then, in tandem with the longwave radiation released by the element (L) being observed from the observatory, the longwave radiation from the sky (L^{sky}) is reflected into the air. Both L^{sky} and L pass through the atmosphere before arriving at the observatory, then together with the longwave radiation emitted by the atmosphere (L^{atm}), transmitting through the window of the housing before reaching the infrared receptor. Along

with other types of radiation, the infrared receptor also captures longwave radiation from the window (L^{win}). The camera output voltage corresponding to U_{ij} combining the relationship defined in Equation 3 and the aforementioned factors could be expressed as the following equation :

$$U_{ij} = \frac{1}{\varepsilon_{ij}\tau_{ij}^{atm}\tau^{win}} U_{ij}^r - \frac{1 - \varepsilon_{ij}}{\varepsilon_{ij}} U^{sky} - \frac{1 - \tau_{ij}^{atm}}{\varepsilon_{ij}\tau_{ij}^{atm}} U^{atm} - \frac{1 - \tau^{win}}{\varepsilon_{ij}\tau_{ij}^{atm}\tau^{win}} U^{win} \quad (6)$$

where ε_{ij} is the thermal emissivity from the element at position ij in the thermal image, τ_{ij}^{atm} is the transmissivity of the atmosphere between the element and the rooftop observatory, and τ^{win} is the transmissivity of the window.

T_{ij} could be calculated through Equation 3 if U_{ij} is known. ε_{ij} and τ^{win} could be estimated from the material properties of the element and the window, respectively. τ_{ij}^{atm} can be calculated from weather data collected from a weather station.

5.2. Weather stations data

The weather information obtained from the weather stations could be used together with the thermal images gathered by the



Figure 6: Weather station locations [19, 18, 17]

Variable	Minimum value	Maximum value
Thermal emissivity (-)	0.7	1.0
Sky temperature (°C)*	11.0	33.0
Air temperature (°C)**	19.0	37.0
Air relative humidity (%)**	30.0	100.0
Distance object (m)	100.0	1000.0
Window temperature (°C)+	20.0	60.0
Window transmittance (-)	0.8	1.0

* The sky temperature ($T^{sky} = g(U^{sky})$) was measured by Miguel et al. [4]

** Weather data recorded by the Meteorological Service of Singapore [23]

+ Measured from a HOBO UX100-014M sensor

Table 4: Constrains of each variable considered during the sensitivity analysis of T_{ij}

rooftop observatory to estimate urban heat fluxes. Air temperature, relative humidity, dew point, wind speed and direction, gust speed, and solar radiation were measured by eight weather stations.

Weather stations near the observatory camera could be used to calculate τ_{ij}^{atm} in the following equation according to Waldemar and Klecha [24, 15]:

$$\tau_{ij}^{atm} = x \cdot \exp[-\sqrt{d_{ij}}(\alpha_1 + \beta_1 \sqrt{\omega})] + (1-x) \cdot \exp[-\sqrt{d_{ij}}(\alpha_2 + \beta_2 \sqrt{\omega})] \quad (7)$$

where d_{ij} is the distance between the element and the observatory at position ij of the thermal image, ω is the atmosphere's water vapor content, α , β , and x are empirical coefficients. ω can be estimated from the air temperature (T_{air}) and relative humidity (ϕ) measured from the weather stations using the following equation:

$$\omega = \phi \cdot \exp[\gamma_0 + \gamma_1 T_{air} + \gamma_2 T_{air}^2 + \gamma_3 T_{air}^3] \quad (8)$$

where γ is another set of empirical coefficients described in Waldemar and Klecha [24, 15]

5.3. Preprocessing

Following the classification of CNN, segmentation of the desired region and extraction of its radiometric data are required in order to evaluate the dataset. Flirextractor python package [25] is recommended, as it allows extracting temperature data from regions of interest in the thermal images and storing it in CSV (comma-separated values) format with a simple process. The temperature data from thermal images were converted using Equation 1. The python package Labelme [26] is helpful in the segmentation of regions of interest for analysis. The relevant codes are provided in the Code availability section.

5.4. Image information

The thermal image data are classified and stored based on the positions they are taken. The image datasets contain information including time, positioning of the device, and locations of the observatory (Kent Vale or S16). The building detail and their surrounding environment could be seen based on the corresponding real images provided in this work. Analysis can be conducted in the time domain, frequency domain, or both, based on the nature of the time series and the degree of information to be retrieved [16].

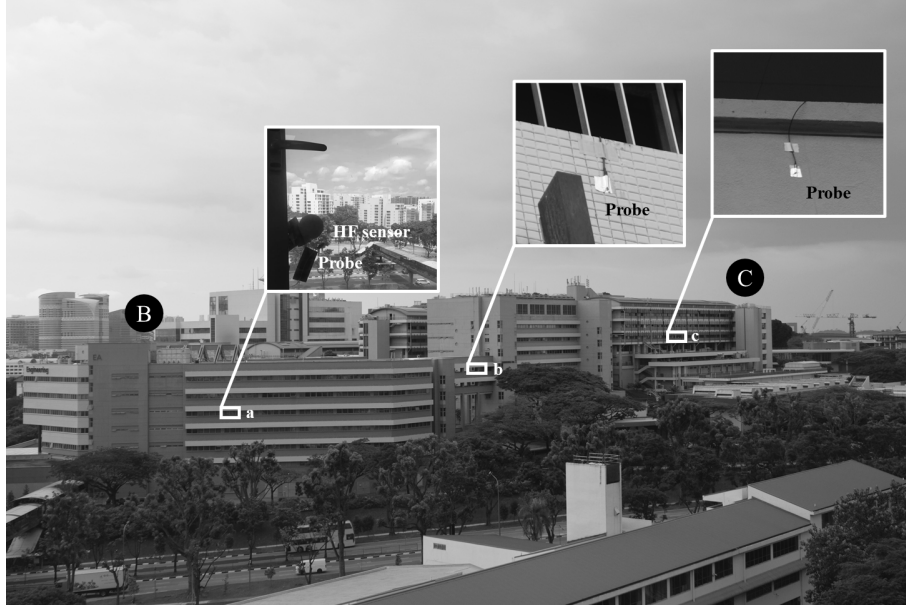


Figure 7: Locations where sensors were placed in to calibrate thermal images and measure the surface temperature [15]

5.5. Potential applications

The thermal images provide surface temperatures of urban elements such as buildings, roads, and vegetation. Some example applications of surface temperature data are urban heat island analysis [15, 27], urban energy monitoring [28], and building thermal performance monitoring [9, 29, 16]. A detailed application of urban observatory is available in Dobler’s work [1]. Thermal images collected by the observatory can provide high-resolution data to study dynamic interactions in buildings at the district scale, which is much smaller compared to the city scale captured by satellite thermal image data, which are used frequently in relevant fields. Further studies of the thermal properties of non-residential buildings can be conducted and compared with those estimated at the city scale. The image data may also be subjected to digital image processing techniques in addition to statistical analysis. While the dataset supplied here is appropriate for the majority of applications, there is still a potential for improvement with regard to the accuracy of the surface temperature measurements. Discussions regarding the data and new approaches to accessing the data are welcomed.

5.6. Privacy and safety control

All these thermal images provided a foundation for the research analysis of living environments in cities. Researchers are encouraged to use various techniques such as computational statistics, machine learning, and sequential analysis to analyze the data. However, data misuse needs to be prevented [1, 30]. Since IoT cameras can be easily abused [31], the dataset collected here should include sufficient privacy protections for relevant individuals, and cities [1, 32]. In such case, the images collected in this work do not contain personally identifiable information [33] such as facial features, and the individual feature cannot be tracked. All taken images were strictly limited

in pixel resolution so that interiors of buildings cannot be seen [1].

6. Code availability

Python 3 was used for data processing and analysis. The simple demonstration of code suggested to use in this work could be found in the following GitHub link: <https://github.com/buds-lab/project-iris-dataset>. The code uses two specific GitHub packages: Flirextractor [25] and Labelme [26]. Flirextractor is an efficient Python package for extracting temperature data from thermal images and converting it into an array, then saving it as a CSV file for further access. The link to the GitHub package describing the usage of Flirextractor in detail is as follows: <https://github.com/aloisklink/flirextractor>. Labelme is a graphical image annotation tool written in Python. It allows users to demarcate the desired area of any shape with simple mouse clicks. Detailed instructions for Labelme can be found at the following link: <https://github.com/wkentaro/labelme>. Please contact the corresponding author directly if you have any particular requirements.

Acknowledgements

This research is supported by the National Research Foundation and the Prime Minister’s Office of Singapore under its Campus for Research Excellence and Technological Enterprise (CREATE) program. It was funded through a grant to the Berkeley Education Alliance for Research in Singapore (BEARS) for the Singapore-Berkeley Building Efficiency and Sustainability in the Tropics (SinBerBEST2) program. BEARS was established by the University of California, Berkeley, as a center for intellectual excellence in research and education in

Singapore. This research is also supported by the Multi-scale Digital Twins for the Urban Environment: From Heartbeats to Cities project, funded by the Singapore Ministry of Education (MOE) Tier 1 Academic Research Fund.

Author contributions statement

S.L. wrote the original draft and assisted in data collection and formal analysis, V.S. and M.M. designed and deployed the data collection platform, P.A. and M.I. supported the data collection process, A.C. and F.B. provided conceptual input for the data platform deployment, K.P. edited and reviewed the manuscript. and C.M. supervised the deployment, data collection, and development of this article. All authors have reviewed the manuscript.

Competing interests

The authors declare no competing interests.

References

- [1] G. Dobler, F. B. Bianco, M. S. Sharma, A. Karpf, J. Baur, M. Ghandehari, J. Wurtele, S. E. Koonin, The urban observatory: a multi-modal imaging platform for the study of dynamics in complex urban systems, *Remote Sensing* 13 (2021) 1426.
- [2] P. Liu, F. Biljecki, A review of spatially-explicit geoai applications in urban geography, *International Journal of Applied Earth Observation and Geoinformation* 112 (2022) 102936.
- [3] Iea (2022), buildings, tracking report, *buildings* <https://www.iea.org/reports/buildings>, 2022.
- [4] M. Miguel, W. N. Hien, I. Marcel, H. D. J. Chung, H. Yueer, Y. Zhongqi, D. Ji-Yu, S. V. Raghavan, N. N. Son, A physically-based model of interactions between a building and its outdoor conditions at the urban microscale, *Energy and Buildings* 237 (2021) 110788.
- [5] E. Lucchi, Applications of the infrared thermography in the energy audit of buildings: A review, *Renewable and Sustainable Energy Reviews* 82 (2018) 3077–3090.
- [6] M. Martin, A. Chong, F. Biljecki, C. Miller, Infrared thermography in the built environment: A multi-scale review, *Renewable and Sustainable Energy Reviews* 165 (2022) 112540.
- [7] A. Ngie, K. Abutaleb, F. Ahmed, A. Darwish, M. Ahmed, Assessment of urban heat island using satellite remotely sensed imagery: a review, *South African Geographical Journal= Suid-Afrikaanse Geografiese Tydskrif* 96 (2014) 198–214.
- [8] C. R. d. Almeida, A. C. Teodoro, A. Gonçalves, Study of the urban heat island (uhi) using remote sensing data/techniques: A systematic review, *Environments* 8 (2021) 105.
- [9] C. A. Balaras, A. Argiriou, Infrared thermography for building diagnostics, *Energy and buildings* 34 (2002) 171–183.
- [10] P. Arjunan, G. Dobler, K. Lee, C. Miller, F. Biljecki, K. Poolla, Operational characteristics of residential air conditioners with temporally granular remote thermographic imaging, in: *BuildSys '21: Proceedings of the 8th ACM International Conference on Systems for Energy-Efficient Buildings, Cities, and Transportation*, Proceedings of the 8th ACM International Conference on Systems for Energy-Efficient Buildings, Cities, and Transportation, pp. 184–187.
- [11] J. F. Sham, T. Y. Lo, S. A. Memon, Verification and application of continuous surface temperature monitoring technique for investigation of nocturnal sensible heat release characteristics by building fabrics, *Energy and Buildings* 53 (2012) 108–116.
- [12] L. W. Chew, X. Liu, X.-X. Li, L. K. Norford, Interaction between heat wave and urban heat island: A case study in a tropical coastal city, singapore, *Atmospheric Research* 247 (2021) 105134.
- [13] M. Roth, Review of urban climate research in (sub) tropical regions, *International Journal of Climatology: A Journal of the Royal Meteorological Society* 27 (2007) 1859–1873.
- [14] M. Ignatius, R. Xu, Y. Hou, X. Liang, T. Zhao, S. Chen, N. Wong, F. Biljecki, Local climate zones: Lessons from singapore and potential improvement with street view imagery, *ISPRS Annals of Photogrammetry, Remote Sensing and Spatial Information Sciences X-4/W2-2022* (2022) 121–128.
- [15] M. Martin, V. Ramani, C. Miller, Infrared investigation in singapore (iris) observatory: Urban heat island contributors and mitigators analysis using neighborhood-scale thermal imaging, 2022.
- [16] V. Ramani, M. Martin, P. Arjunan, A. Chong, K. Poolla, C. Miller, Longitudinal thermal imaging for scalable non-residential hvac and occupant behaviour characterization, 2022.
- [17] S. Chen, N. H. Wong, M. Ignatius, W. Zhang, Y. He, Z. Yu, D. J. C. Hii, Atlas: Software for analysing the relationship between urban microclimate and urban morphology in a tropical city, *Building and Environment* 208 (2022) 108591.
- [18] Z. Yu, S. Chen, N. H. Wong, M. Ignatius, J. Deng, Y. He, D. J. C. Hii, Dependence between urban morphology and outdoor air temperature: A tropical campus study using random forests algorithm, *Sustainable Cities and Society* 61 (2020) 102200.
- [19] 1°17'50"N, 103°46'37"E. **Google Earth**. march 05, 2016. november 01, 2022, <https://earth.google.com/web/@1.29728934,103.77702845,23.33038212a,2430.67786248d,35y,27.55033278h,0t,0r>, 2016.
- [20] S. Lin, V. Ramani, M. Martin, P. Arjunan, A. Chong, F. Biljecki, M. Ignatius, K. Poolla, C. Miller, Infrared investigation in singapore (iris) dataset, *Zenodo* <https://doi.org/10.5281/zenodo.7463996>, 2022.
- [21] I. M. Sobol, Global sensitivity indices for nonlinear mathematical models and their monte carlo estimates, *Mathematics and computers in simulation* 55 (2001) 271–280.
- [22] A. Saltelli, P. Annoni, I. Azzini, F. Campolongo, M. Ratto, S. Tarantola, Variance based sensitivity analysis of model output. design and estimator for the total sensitivity index, *Computer physics communications* 181 (2010) 259–270.
- [23] Historical daily records, 2022., *climate-historical-daily* <http://www.weather.gov.sg/climate-historical-daily>, 2022.
- [24] M. Waldemar, D. Klecha, Modeling of atmospheric transmission coefficient in infrared for thermovision measurements, in: *Proceedings of the Sensor*, pp. 903–907.
- [25] aloisklink/flirextractor v1.0.2: An efficient gplv3-licensed python package for extracting temperature data from flir irt images., *flirextractor* <https://github.com/aloisklink/flirextractor>, 2020.
- [26] B. C. Russell, A. Torralba, K. P. Murphy, W. T. Freeman, Labelme: a database and web-based tool for image annotation, *International journal of computer vision* 77 (2008) 157–173.
- [27] Q. Weng, D. A. Quattrochi, Urban remote sensing, CRC press, 2018.
- [28] X. X. Yang, Urban remote sensing: Monitoring, synthesis and modeling in the urban environment, John Wiley & Sons, 2021.
- [29] A. Kylili, P. A. Fokaides, P. Christou, S. A. Kalogirou, Infrared thermography (irt) applications for building diagnostics: A review, *Applied Energy* 134 (2014) 531–549.
- [30] L. Floridi, J. Cows, M. Beltrametti, R. Chatila, P. Chazerand, V. Dignum, C. Luetge, R. Madelin, U. Pagallo, F. Rossi, et al., Ai4people—an ethical framework for a good ai society: Opportunities, risks, principles, and recommendations, *Minds and machines* 28 (2018) 689–707.
- [31] M. Tom Yeh, et al., Designing a moral compass for the future of computer vision using speculative analysis, in: *Proceedings of the IEEE Conference on Computer Vision and Pattern Recognition Workshops*, pp. 64–73.
- [32] Privacy, Big Data, and the Public Good: Frameworks for Engagement, Cambridge University Press, 2014.
- [33] E. McCallister, Guide to protecting the confidentiality of personally identifiable information, volume 800, Diane Publishing, 2010.